Supplemental data for

Heteroblastic Development of Transfer Cells in Arabidopsis is Controlled by the miR156/*SPL* Module

Suong T. T. Nguyen, Teighan Greaves and David W. McCurdy

This PDF file includes:

Supplemental Figure S1. Confocal images of five classes of PP and PP TCs based on wall ingrowth abundance.

Supplemental Figure S2. Heteroblastic variations in three ecotypes Col-0, Ws-2 and L*er*-0.

Supplemental Figure S3. Rejuvenation of internal anatomical traits in leaf 10 upon prolonged defoliation.

Supplemental Figure S4. Confocal imaging of tracheary elements in mature leaf veins.

Supplemental Figure S5. Heteroblastic features of Col-0 plants grown under short-day conditions.

Supplemental Figure S6. Effects of *sqn-6* on VPC traits.

Supplemental Figure S7. Leaf morphology of *35S::MIM156* and *35S::MIR156a* transgenic lines.

Supplemental Figure S8. Leaf morphology and leaf position at which abaxial trichomes were first produced in Col-0, *zip*, *rdr6* and *sgs3* plants.

Supplemental Table S1. Variations on number of abaxial trichomes and total leaf number of *35S::MIM156* transgenic line.

Supplemental Table S2. List of primers used for RT-qPCR.

Supplemental Materials and Methods. Real-time quantitative RT-PCR.

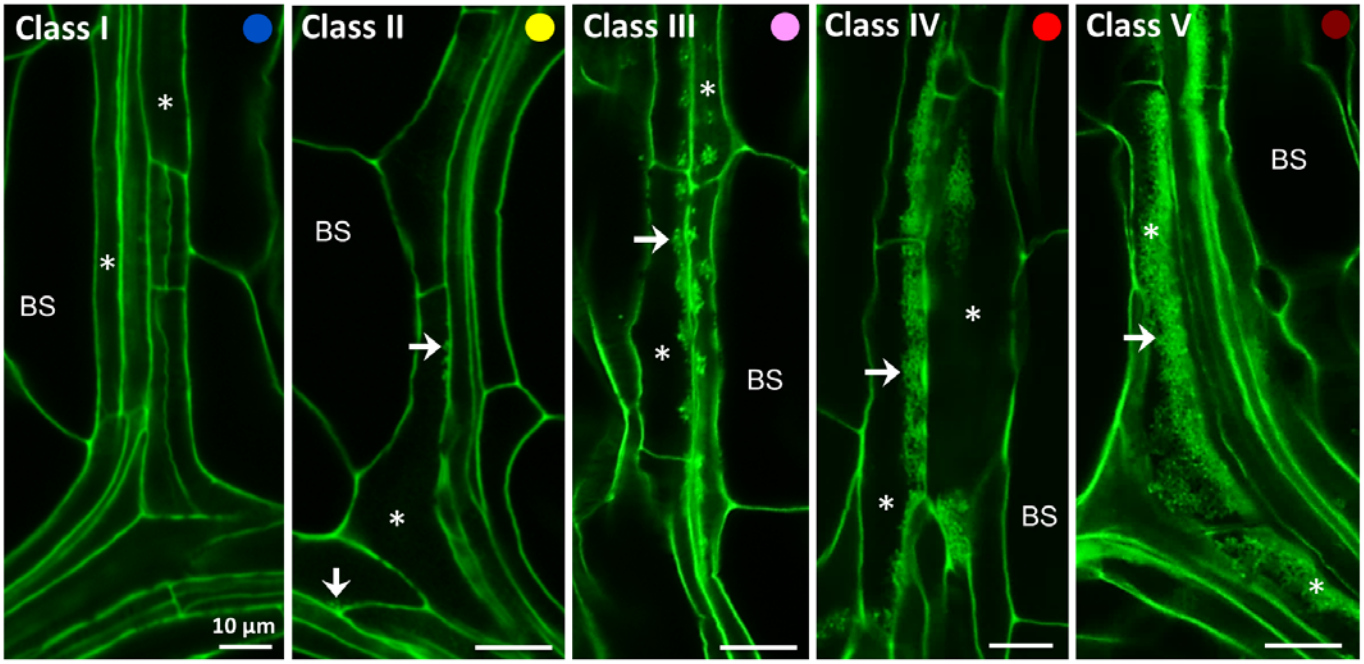

Supplemental Figure S1. Confocal images of the five classes of PP or PP TCs based on extent of wall ingrowth deposition. Class I (●, 0 points) – no wall ingrowths; Class II (●, 2 points) – first evidence of discrete, punctate or linear regions of wall ingrowths appearing in some PP cells, defining them as PP TCs, in the field of view; Class III (●, 4 points) – more substantial clusters of wall ingrowths are evident, as shown here, or alternatively, more substantial linear regions of ingrowth deposition along the wall of the PP TC, typically occurring in all PP TCs in the field of view; Class IV (●, 6 points) – extensive levels of wall ingrowths appearing as a continuous thick band of deposition along the wall of all PP TCs; Class V (●, 8 points) – massive levels of wall ingrowth deposition that project into and occupy a considerable volume of each PP TC in the field of view. BS, bundle sheath. Asterisks indicate PP cells or PP TCs; arrows point to wall ingrowths. Scale bars = 10 µm for all images.

A

Ecotype / Leaf	Col-0	Ws-2	L*er*-0
1 & 2	0	0	0
3	0	0.7 ± 1.1	0
4	0	9.0 ± 9.2	0.8 ± 1.3
5	0.3 ± 0.8	21.4 ± 13.9	1.1 ± 0.9
6	2.7 ± 3.5	47.0 ± 18.7	11.6 ± 9.4
7	9.6 ± 9.1	119.0 ± 36.8	36.0 ± 26.5
8	17.0 ± 11.0		
9	31.4 ± 18.2		
10	53.1 ± 26.5		
11	113.1 ± 88.0		
12	137.4 ± 51.3		
Total leaf number	10.8 ± 0.9	6.6 ± 0.5	6.6 ± 0.7

B

Diameter of PP cells/PP TCs (µm)	Leaf 1	Leaf 6	Leaf 11
Tip	7.9 ± 0.3	6.5 ± 0.1	5.6 ± 0.1
Middle	7.5 ± 0.4	7.1 ± 0.3	4.5 ± 0.3
Base	8.3 ± 0.1	6.6 ± 0.3	4.4 ± 0.2

C

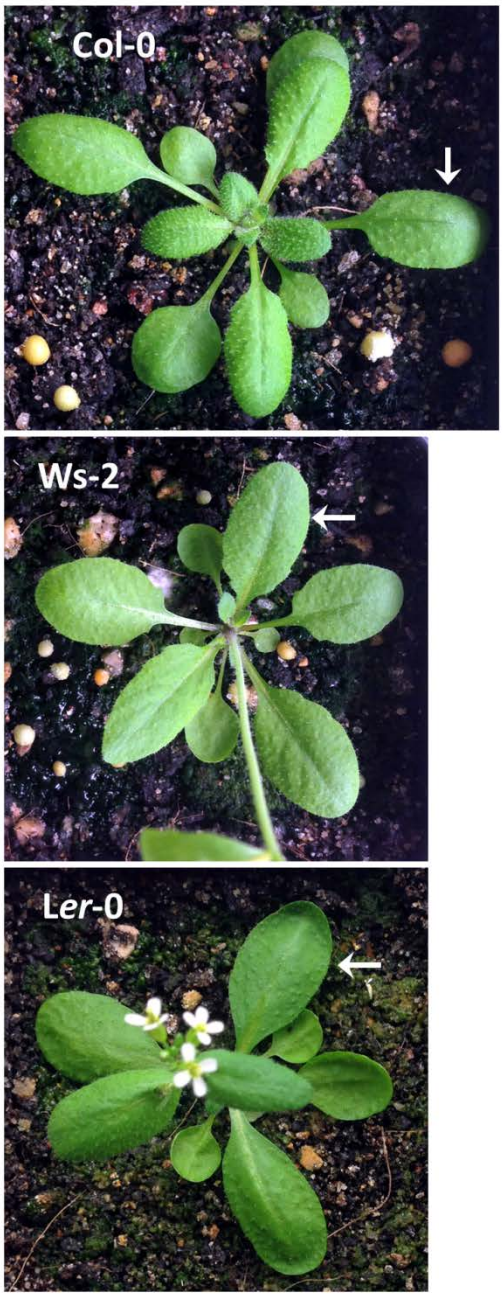

Supplemental Figure S2. Heteroblastic variations in three ecotypes Col-0, Ws-2 and L*er*-0. A, Numbers of abaxial trichomes in individual leaves and total leaf number in Col-0 (*n* = 18), Ws-2 (*n* = 7) and L*er*-0 (*n* = 9) plants. Data represents mean ± SD. B, Diameter of PP cells or PP TCs measured at tip, middle and base regions of juvenile leaf 1 (60 cells measured in total from 3 leaves), transition leaf 6 (60 cells measured in total from 3 leaves) and adult leaf 11 (146 cells measured in total from 9 leaves) from Col-0 plants. Data is mean ± SE. C, Mature leaf 6 (arrows) in 25-day-old Col-0, 25-day-old Ws-2 and 28-day-old L*er*-0 plants.

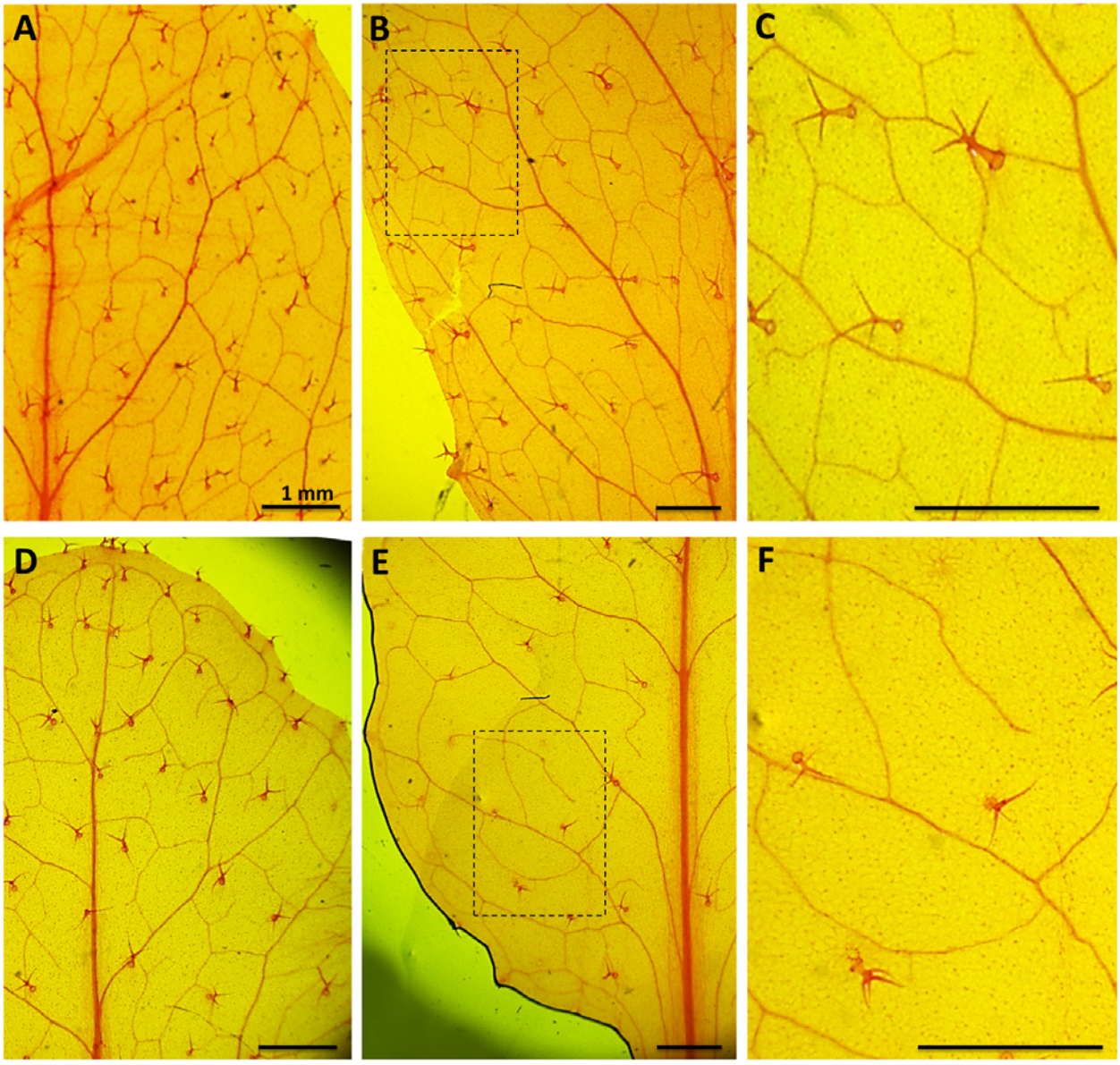

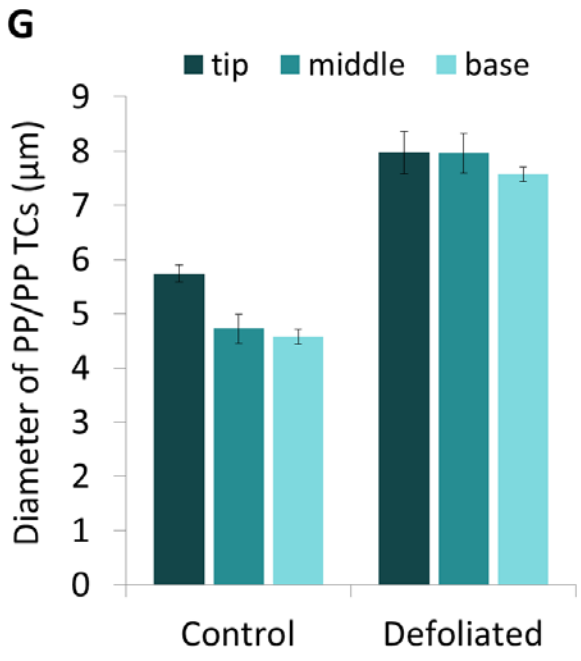

Supplemental Figure S3. Rejuvenation of internal anatomical traits in leaf 10 upon prolonged defoliation. A to C, mPS-PI-stained adult leaf 10 of control plants shows complex venation patterns; C, Higher magnification view of boxed region in B. D to F, mPS-PI stained rejuvenated leaf 10 of defoliated plants shows simple venation patterns; F, Higher magnification view of boxed region in D. Scale bars = 1 mm for all images. G, Diameter of PP cells or PP TCs measured at tip, middle and base regions of leaves shown in A (54 cells measured in total from 3 leaves) and B (96 cells measured in total from 5 leaves). Data is mean ± SE.

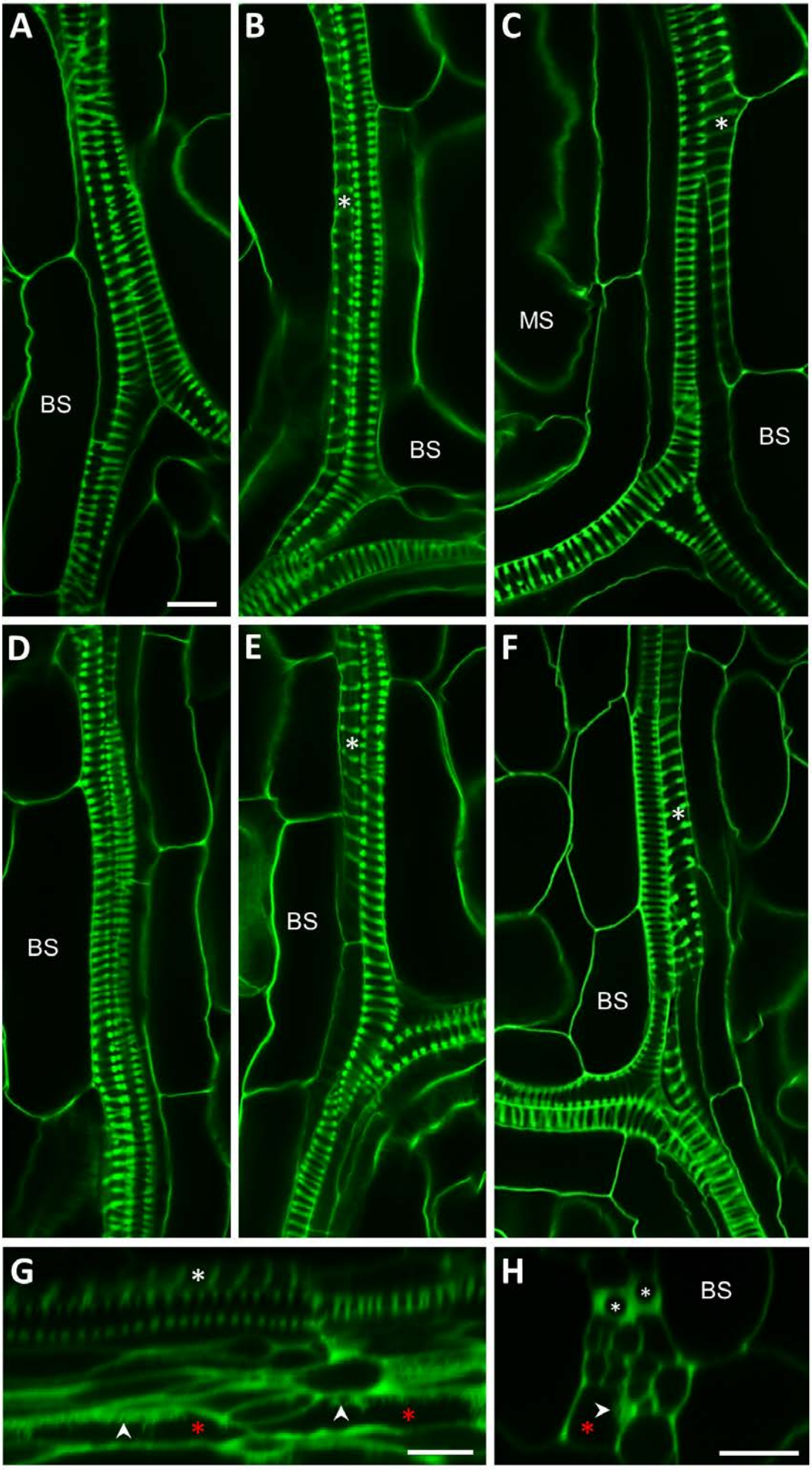

Supplemental Figure S4 (see legend on next page).

Supplemental Figure S4. Confocal imaging of tracheary elements in mature leaf veins. These images revealed no major differences in xylem development in mature juvenile leaves (A and B), mature transition leaves (C, G and H) and mature adult leaves (D to F). In minor veins of these leaves xylem was frequently comprised of two, and occasionally three, tracheary elements as revealed by single confocal sections (A to F), and x-z (G) and y-z (H) projections of a confocal z-stack. These tracheary elements were typical of protoxylem vessels with helical and annular thickenings. White asterisks in B, C, E, F and G indicate tracheary elements which were probably formed earlier during xylem development as indicated by the greater spacing of secondary wall thickenings compared to its neighboring tracheary element. White asterisks in H indicate two tracheary elements in a transverse view reconstructed from a series of confocal z-scans. Red asterisks in G and H indicate PP TCs with abundant wall ingrowth deposition (arrowheads). BS, bundle sheath; Scale bar = 10 μm for A-F, and 10 μm for G and H.

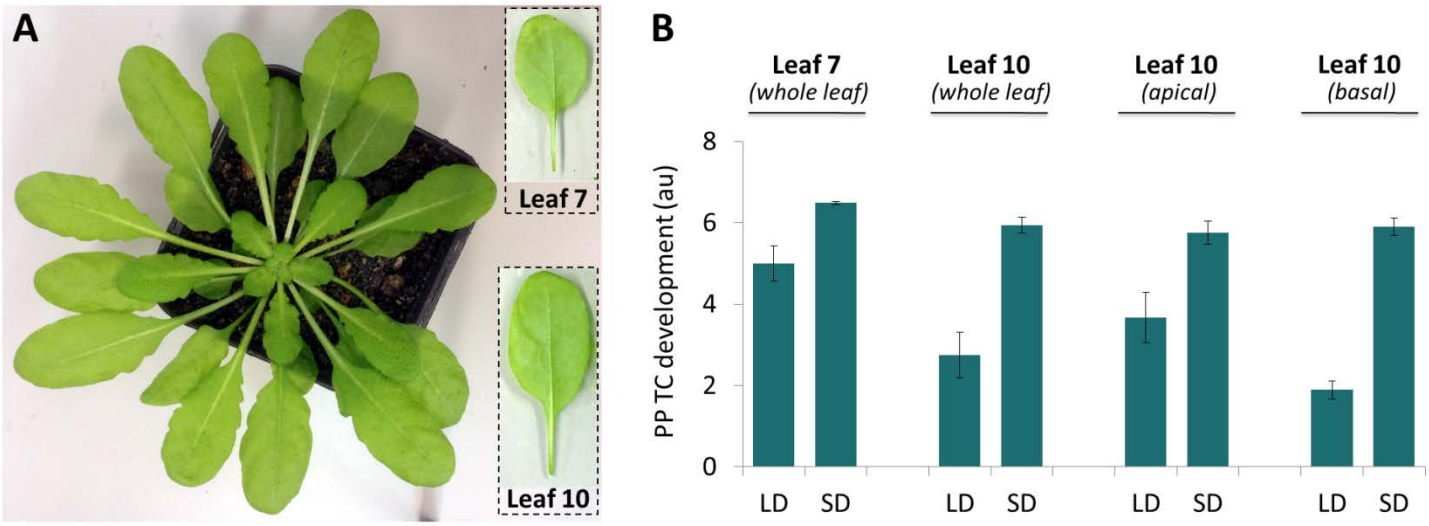

Supplemental Figure S5. Heteroblastic features of Col-0 plants grown under short-day conditions. A, Eight-week-old Col-0 plants; the insets showing the abaxial surface of leaves 7 and 10 (bearing no abaxial trichomes as observed by dissecting microscope). B, PP TC development in leaves 7 and 10 increased compared to that in long-day plants, and resembled PP TC development in leaf 4 or 5, or leaf 5 or 6, respectively, of long-day plants. Analysis of leaf 10 in short-day plants also shows no differences in PP TC development at the base vs tip of the leaf. Data is mean ± SE. n = 3 for leaf 7 and n = 4 for leaf 10.

A

Leaf / Plant	1	2	3	4	5	6	7	Total leaf number
1	0	0	0	0	5	24		6
2	0	0	0	3	9	85		6
3	0	0	0	0	6	41	125	7
4	0	0	1	14				4
5	0	0	0	1	8	12		6
6	0	0	0	0	4	32		6
7	0	0	0	0	7	14	78	7
8	0	0						2

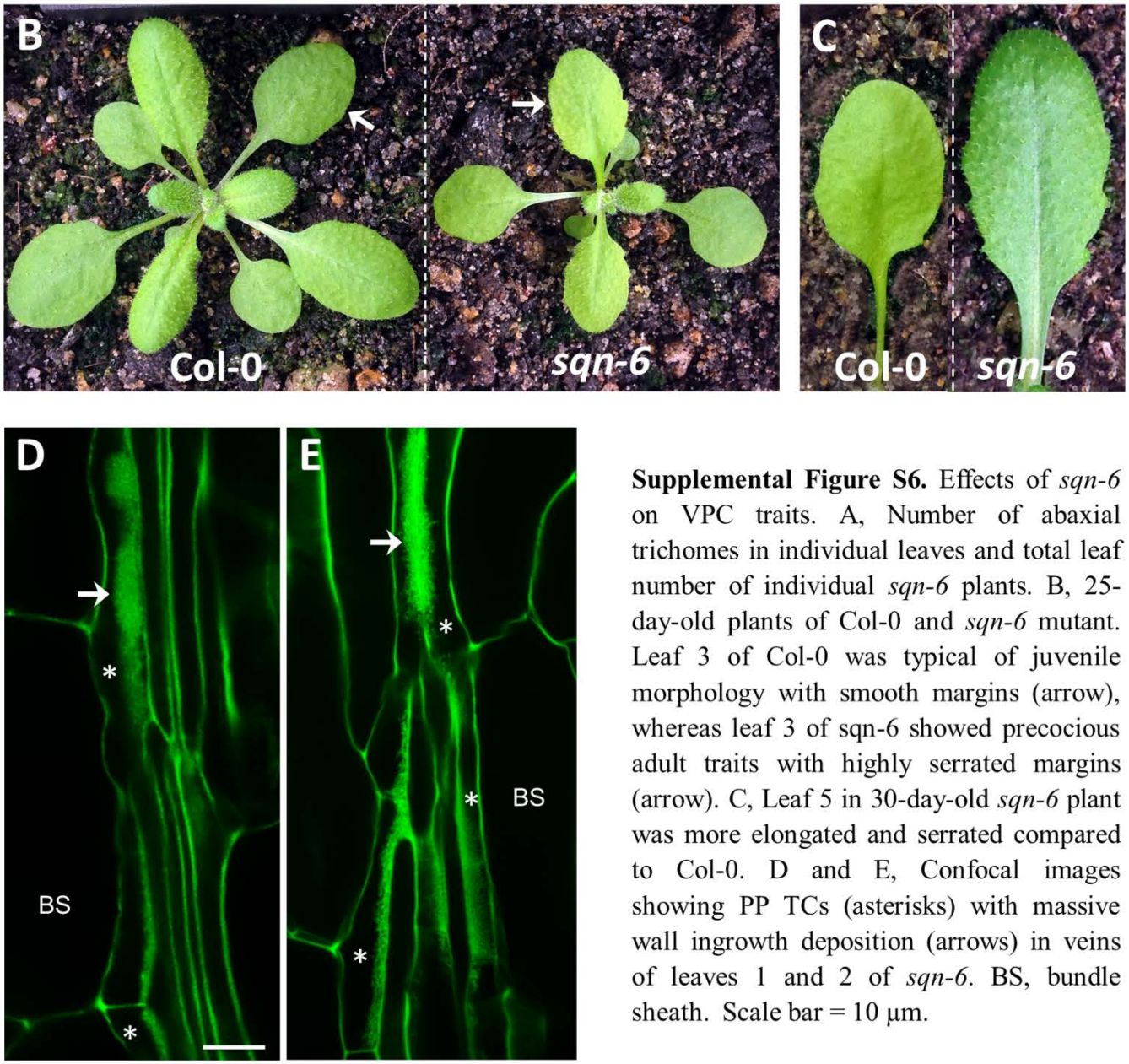

Supplemental Figure S6. Effects of *sqn-6* on VPC traits. A, Number of abaxial trichomes in individual leaves and total leaf number of individual *sqn-6* plants. B, 25-day-old plants of Col-0 and *sqn-6* mutant. Leaf 3 of Col-0 was typical of juvenile morphology with smooth margins (arrow), whereas leaf 3 of sqn-6 showed precocious adult traits with highly serrated margins (arrow). C, Leaf 5 in 30-day-old *sqn-6* plant was more elongated and serrated compared to Col-0. D and E, Confocal images showing PP TCs (asterisks) with massive wall ingrowth deposition (arrows) in veins of leaves 1 and 2 of *sqn-6*. BS, bundle sheath. Scale bar = 10 μm.

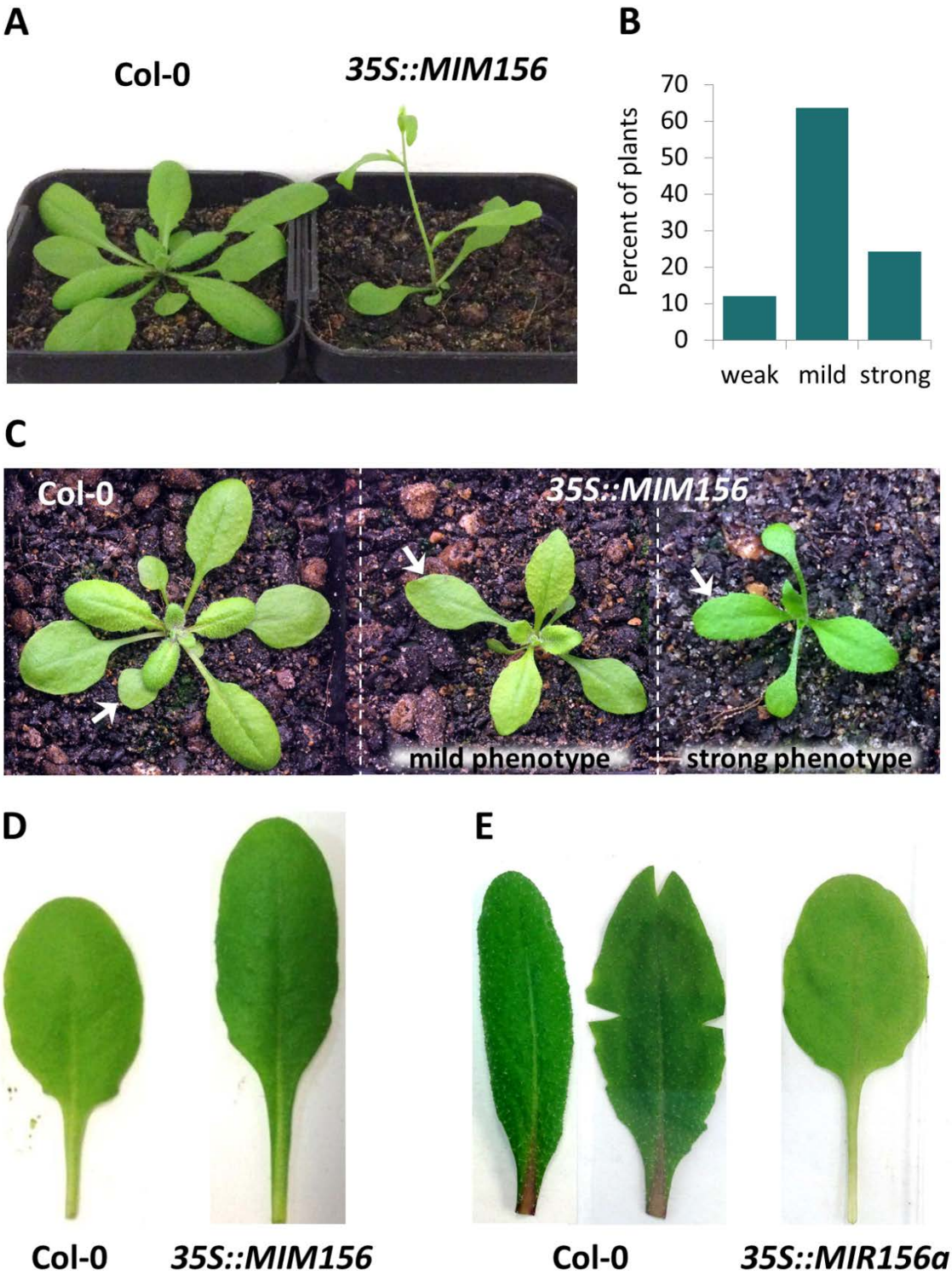

Supplemental Figure S7. Leaf morphology of *35S::MIM156* and *35S::MIR156a* transgenic lines. A, 27-day-old Col-0 and *35S::MIM156* plants. B, Percent of *35S::MIM156* plants having 2-4 leaves (strong phenotype), 5-7 leaves (mild phenotype) and 8-9 leaves (weak phenotype); *n* = 71. C, 24-day-old plants of Col-0 and *35S::MIM156*; arrows point to leaf 1 or 2. D, Leaf 5 from 30-day-old Col-0 and *35S::MIM156* plants. E, Leaf 10 from 35-day-old Col-0 and *35S::MIR156a* plants. Images of leaf 10 from Col-0 were taken before and after the leaf being flattened to reveal leaf margins.

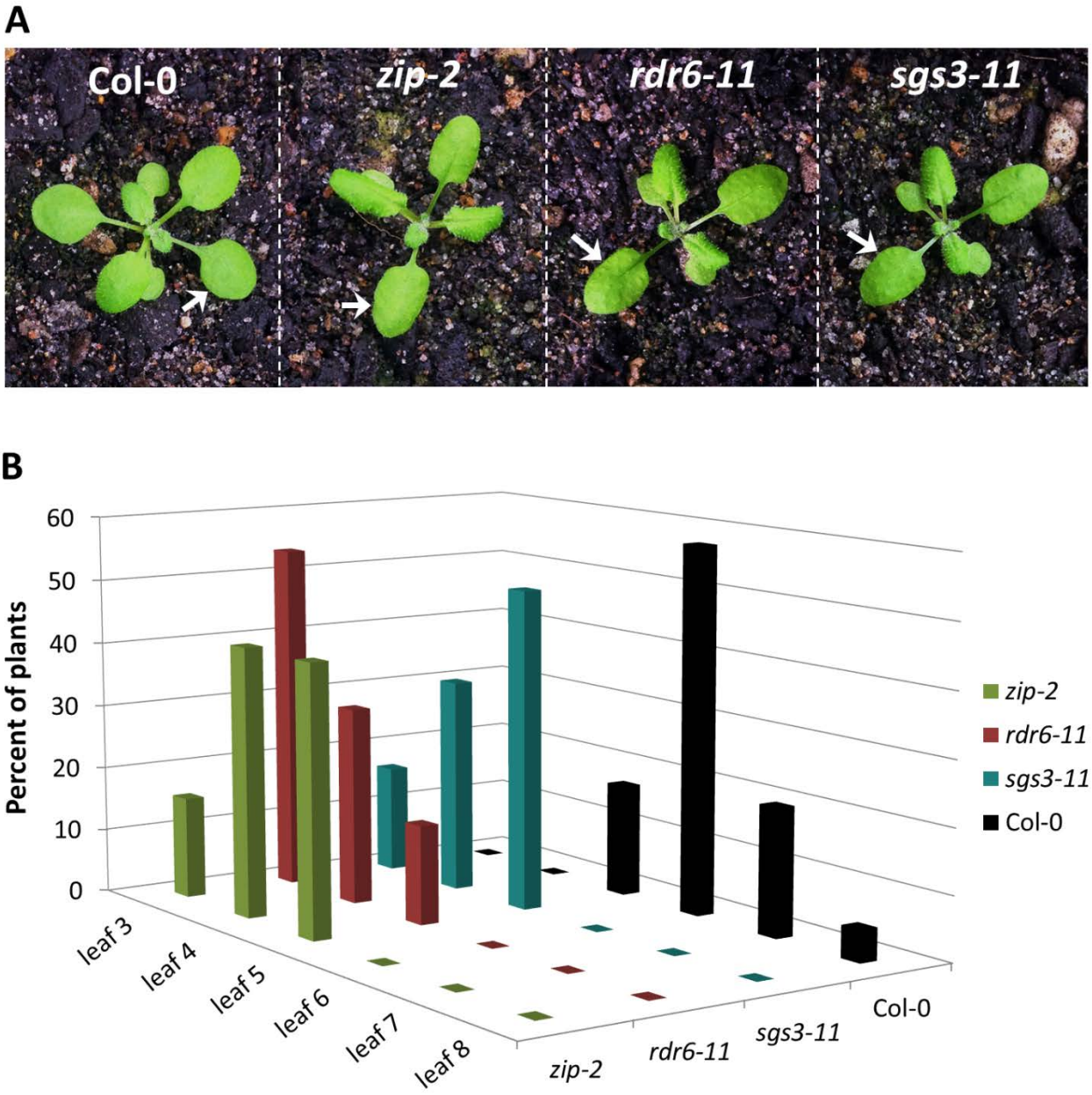

Supplemental Figure S8. Leaf morphology and leaf position at which abaxial trichomes were first produced in Col-0, *zip-2*, *rdr6-11* and *sgs3-11* plants. A, 15-day-old Col-0, *zip-2*, *rdr6-11* and *sgs3-11* plants; arrows point to leaf 1 or 2. B, Frequency distribution for the position of the earliest leaf bearing abaxial trichomes. In these plants the earliest leaf having abaxial trichomes was most frequently leaf 6 in Col-0, leaf 4 and 5 in *zip-2*, leaf 3 in *rdr6-11* and leaf 5 in *sgs3-11*.

Supplemental Table S1. Variations on number of abaxial trichomes and total leaf number of *35S::MIM156* transgenic line.

Leaf / Plant	1	2	3	4	5	6	7	Total leaf number
1	44	38	75					3
2	24	27	55					3
3	15	15	20	36				4
4	18	22	87	29				4
5	14	10	10	16	25			5
6	17	18	17	28	54			5
7	4	1	7	11	35			5
8	4	2	0	7	46			5
9	17	31	49	36	123			5
10	6	4	0	3	12	48		6
11	12	12	10	24	43	97		6
12	15	17	12	29	41	102		6
13	12	11	7	9	30	32		6
14	3	8	0	0	2	16	38	7
15	6	3	3	5	12	25	70	7
16	13	15	7	6	10	10	55	7

Supplemental Table S2. List of primers used for RT-qPCR. ^ indicates position of an exon-exon junction.

Arabidopsis gene ID	Annotation	5' →3' Primer Sequences (F/R)	Tm (°C)	Amplicon length (bp)	Distance from 3' end (bp)
AT2G20790	Clathrin adaptor complexes medium subunit family protein	GTCGGGGCATCTGTATCTCG	60.04	102	288
		CCCTGAAGTCAC^CTGAGCAG	60.04		
AT2G19950	Golgin candidate 1	TACACCGACTCCAG^GAGCAA	60.54	60	279
		AAACGTTGTTGGTCATTGCCG	60.54		
AT1G76940	RNA-binding (RRM/RBD/RNP motifs) family protein	GCGCCTTACAAG^GCTATCGAA	60.81	67	322
		GAAAACTGGAGCCGCAGGAA	60.89		
AT1G79810	Peroxin 2	CCTTGTCAGCACAG^GTACTGTT	60.49	101	452
		TGTATGGCAACCACAGGCTC	60.32		
AT2G33810	SPL3	TGGACACAACGAGAGAAGGC	59.97	74	210
		CCTTCAAACCGGGATCTCACA	60.00		
AT2G42200	SPL9	GGCAATGGGTGAGTTCGAGT	60.32	79	218
		AGCCCTTGTGTTCTCATCTTCC	60.29		
AT1G27370	SPL10	ACTTCCAGACAAAGGT^GTGGG	60.13	120	302
		ACGGGAGTGTGTTTGATCCC	59.96		
AT3G57920	SPL15	TCTCGGAGCCAGCAGATTTC	59.82	111	170
		CTCTTGTGTTCTCGGGTTCCA	59.93		
	U6 (Forward)	GGAACGATACAGAGAAGATTAGCA	58.17	NA	NA
	miR156 (Forward)	GCGCCTGACAGAAGAGAGTG	60.74	NA	NA
	miR172 (Forward)	GCGCGAGAATCTTGATGATGC	60.40	NA	NA
	Universal Reverse	CAGTGCAGGGTCCGAGGTA	60.98	NA	NA
	U6 (RT)	CCAGTGCAGGGTCCGAGGTATTTGG ACCATTTCTCGAT	NA	NA	NA
	miR156 (RT)	GTCGTATCCAGTGCAGGGTCCGAGG TATTCGCACTGGATACGACGTGCTC	NA	NA	NA
	miR172 (RT)	GTCGTATCCAGTGCAGGGTCCGAGG TATTCGCACTGGATACGACATGCAG	NA	NA	NA

Supplemental Materials and Methods: Real-time quantitative RT-PCR

Identification and validation of novel reference genes for quantification of mRNAs in Arabidopsis leaf tissue

We used the method of Hruz et al. (2011) to identify suitable reference genes for normalization of mRNA expression specifically across maturation of juvenile and adult leaf tissue. We selected potential reference genes based on public microarray data using RefGenes, available within Genevestigator (https://www.genevestigator.com). From the 10615 Arabidopsis microarray datasets available in Genevestigator, we chose a set of 57 microarrays from 8 independent studies, in which the experimental conditions were as similar as possible to the experiments performed in this study. To minimize the effects of variation in amplification efficiencies between reference genes and target genes on the accuracy of qPCR results (Czechowski et al., 2005; Bustin et al., 2009; Svec et al., 2015), we defined the range of reference gene expression to be in the same expression range of our target genes, namely *SPL3*, *SPL9*, *SPL10* and *SPL15*. With these two criteria defined for RefGenes, Genevestigator returned the top 20 probe sets with the lowest variance, from which we chose *AT1G76940* (RNA-binding (RRM/RBD/RNP motifs) family protein), *AT1G79810* (PEROXIN 2), *AT2G19950* (GOLGIN CANDIDATE 1) and *AT2G20790* (clathrin adaptor complexes medium subunit family protein), all of which appear in the list of the 100 most stably expressed genes across various developmental series in Arabidopsis (see Czechowski et al., 2005). To empirically validate these potential reference genes, we performed RT-qPCR and used geNorm (Vandesompele et al., 2002) and NormFinder (Andersen et al., 2004) algorithms to assess expression stability. Analyses by these two algorithms returned *AT1G79810* and *AT2G20790* as the most stably expressed genes across all our leaf samples, namely leaves from Col-0 at different developmental stages and from transgenic lines used in this study.

RT-qPCR primer design, specificity and efficiency

qPCR primers for mRNAs were designed using Primer-BLAST software (Ye et al., 2012) with the following criteria: T_M of 60^{o}C ± 1^{o}C, PCR amplicon lengths of 60 to 150 bp, and at least one primer of a pair bridging an exon-exon junction if possible to prevent amplification of potentially contaminating genomic DNA. As Oligo (dT) primers were used for cDNA synthesis, qPCR primers were also designed to amplify close to the annotated 3' end of mRNAs (see Supplemental Table S2). *In silico* specificity screen of these primers was also performed by Primer-BLAST. Forward primers and universal reverse primers for miR156,

miR172 and U6 were designed according to Varkonyi-Gasic et al. (2007), Kramer et al. (2011), Turner et al. (2013) and with modifications.

Specificity of amplicons was verified by (i) gel-electrophoretic analysis, (ii) melting-curve analysis post-amplification, and (iii) *in silico* prediction of amplicon melting temperature using OligoAnalyzer 3.1 (http://sg.idtdna.com/calc/analyzer). Primer efficiency was assessed for each primer pair in each experiment and listed as following: *AT1G79810*: 95% ± 1.8 (n = 6); *AT2G20790*: 91% ± 3.7 (n = 4); *SPL3*: 88% ± 1.7 (n = 5); *SPL9*: 95% ± 2.2 (n = 5); *SPL10*: 96% ± 1.6 (n = 4); *SPL15*: 97% ± 1.8 (n = 5); U6: 93% ± 1.0 (n = 6); miR156: 91% ± 1.8 (n = 6); miR172: 85% ± 3.1 (n = 4). Data is mean ± SE.

Sample acquisition, total RNA extraction and quality assessment

At two hours into the light period of plant growth, leaf blades (not including petioles) were removed from plants and immediately snap-frozen in liquid nitrogen and stored at -80^{o}C. Total RNA was extracted from these leaves using TRIzol reagent (Life Technologies) according to the manufacturer's protocol and with in-house optimization of the procedures. RNA concentration was measured using a NanoDrop ND-1000 with two or three technical replicates for each RNA sample. On average, 100 mg of ground plant material from juvenile or adult leaves yielded of ~25 or ~70 µg total RNA, respectively. The purity of RNA was estimated by 260/280 and 260/230 ratios. On average, 260/280 ratios were in the range of 1.9-2, and 260/230 ratios were in the range of 2.2-2.5, indicating highly purified RNA. RNA integrity was confirmed by standard agarose gel electrophoresis, showing highly intact RNA (evidenced by intact 28S rRNA, 18S rRNA, 5S/sRNA bands and the presence of clear cytosolic and plastidic ribosomal RNA bands (Box et al., 2011) and the visible absence of genomic DNA contamination.

First strand cDNA synthesis using oligo (dT)$_{18}$ and miRNA-specific stem-loop primers

cDNA synthesis was performed with the RevertAid First Strand cDNA synthesis kit (Thermo Scientific). To minimize variations in cDNA synthesis efficiencies between miR156, miR172 and U6, and between miR156 and its *SPL* target genes, we employed the protocol of Speth and Laubinger (2014) to perform a multiplexed cDNA synthesis of miR156, miR172, U6 and mRNAs. Stem-loop primers were used for cDNA synthesis of miR156, miR172 and U6 and designed according to Varkonyi-Gasic et al. (2007), Kramer et al. (2011), Turner et al. (2013) and with modifications (Supplemental Table S2). Oligo (dT)$_{18}$ was used for priming cDNA synthesis from mRNA.

Prior to cDNA synthesis, total RNA was treated with DNaseI (Thermo Scientific) according to the manufacturer's protocol to remove residual genomic DNA. Between 0.5-1.8 µg DNase-treated total RNA was used in a 20-µl RT reaction. Briefly, 1 µl of 100 µM oligo $(dT)_{18}$ and 0.5 µl of the stem-loop primer mixture (2 µM each primer) were added to DNase-treated total RNA and samples were incubated for 5 min at 65^{o}C. Then 4 µl of 5x RT Buffer, 2 µl of 10 mM dNTPs, 20 units of Ribo-LOCK RNase Inhibitor and 200 units of RevertAid Reverse Transcriptase (RT) (Thermo Scientific) were added to primed-RNA samples. The RT reaction was perform with thermocycling conditions of 30 min at 16°C, followed by pulsed RT of 60 cycles of 30°C for 30s, 42°C for 30s and 50°C for 1s, followed by 85°C for 5 min to inactivate the RT. RT-minus reactions were performed for each corresponding RT-plus sample, and a negative control (NTC) and a positive control (provided by Thermo Scientific) were included in each experiment.

qPCR conditions and analysis

qPCR reactions were performed using a Rotor-Gene 6000 instrument (Qiagen) in technical duplicate for each biological replicate (n = 3-5). The cDNA equivalent of 7.5 ng of total RNA was used in a 10-µl PCR reaction, with the following components added: 5 µl of Maxima SYBR Green qPCR Master Mix 2x (Thermo Scientific), forward and reverse primers to the final concentration of 400 nM each, and nuclease-free water to a total volume of 10 µl. Samples were incubated at 95^{o}C for 10 min, followed by a three step amplification by 40 cycles of 95^{o}C for 10s, 57^{o}C for 30s and 72^{o}C for 20s. Melting curve analysis was performed post-amplification with a ramp from 60^{o}C to 95^{o}C, increasing in increments of 1^{o}C each 5 seconds. Serial 1:2 or 1:3 dilutions of cDNA were employed to create standard curves and subsequently calculate qPCR efficiency.

The quantitative cycle (Cq) was determined using the Cy0 method (Guescini et al., 2008, 2013; Sisti et al., 2010), which is ranked as the best publicly available curve analysis method in terms of algorithm precision, bias and resolution (Ruijter et al., 2013). Raw fluorescence data from each qPCR run was uploaded into the Cy0 website (http://www.cy0method.org/) and the Cy0 team analyzed and returned Cq values. These Cq values were subsequently used in all calculations, including (i) confirmation of the absence and/or no effects (if present) of contaminating genomic DNA (by RT-minus reactions) and primer-dimers (by NTC reactions), (ii) standard-curve analysis to calculate qPCR efficiency, (iii) evaluating the stability of reference genes, and (iv) the Livak formula (Livak and Schmittgen, 2001) to calculate relative abundance levels of transcripts of interest.

References

Andersen CL, Jensen JL, Orntoft TF (2004) Normalization of real-time quantitative reverse transcription-PCR data: a model-based variance estimation approach to identify genes suited for normalization, applied to bladder and colon cancer data sets. Cancer Res **64:** 5245–5250

Box MS, Coustham V, Dean C, Mylne JS (2011) Protocol: A simple phenol-based method for 96-well extraction of high quality RNA from Arabidopsis. Plant Methods **7:** 7

Bustin SA, Benes V, Garson JA, Hellemans J, Huggett J, Kubista M, Mueller R, Nolan T, Pfaffl MW, Shipley GL, et al (2009) The MIQE guidelines: minimum information for publication of quantitative real-time PCR experiments. Clin Chem **55:** 611–622

Czechowski T, Stitt M, Altmann T, Udvardi MK, Scheible WR (2005) Genome-wide identification and testing of superior reference genes for transcript normalization in Arabidopsis. Plant Physiol **139:** 5–17

Guescini M, Sisti D, Rocchi MBL, Stocchi L, Stocchi V (2008) A new real-time PCR method to overcome significant quantitative inaccuracy due to slight amplification inhibition. BMC Bioinformatics **9:** 326

Guescini M, Sisti D, Rocchi MBL, Panebianco R, Tibollo P, Stocchi V (2013) Accurate and precise DNA quantification in the presence of different amplification efficiencies using an improved Cy0 method. PLoS ONE **8:** e68481

Hruz T, Wyss M, Docquier M, Pfaffl MW, Masanetz S, Borghi L, Verbrugghe P, Kalaydjieva L, Bleuler S, Laule O, et al (2011) RefGenes: identification of reliable and condition specific reference genes for RT-qPCR data normalization. BMC Genomics **12:** 156

Kramer MF (2011) Stem-loop RT-qPCR for miRNAs. Curr Protoc Mol Biol Chapter 15: Unit 15.10.

Livak KJ, Schmittgen TD (2001) Analysis of relative gene expression data using real-time quantitative PCR and the $2^{-\Delta\Delta CT}$ method. Methods **25:** 402–408

Ruijter JM, Pfaffl MW, Zhao S, Spiess AN, Boggy G, Blom J, Rutledge RG, Sisti D, Lievens A, De Preter K, et al (2013) Evaluation of qPCR curve analysis methods for reliable biomarker discovery: Bias, resolution, precision, and implications. Methods **59:** 32–46

Sisti D, Guescini M, Rocchi MBL, Tibollo P, D'Atri M, Stocchi V (2010) Shape based kinetic outlier detection in real-time PCR. BMC Bioinformatics **11:** 186

Speth C, Laubinger S (2014) Rapid and parallel quantification of small and large RNA species. Methods Mol Biol. *In* D Staiger, ed, Plant Circadian Networks: Methods and Protocols, Methods in Molecular Biology. Springer, New York, vol. 1158, pp 93–106.

Svec D, Tichopad A, Novosadova V, Pfaffl MW, Kubista M (2015) How good is a PCR efficiency estimate: Recommendations for precise and robust qPCR efficiency assessments. Biomol Detect Quantif **3:** 9–16

Turner M, Adhikari S, Subramanian S (2013) Optimizing stem-loop qPCR assays through multiplexed cDNA synthesis of U6 and miRNAs. Plant Signal Behav **8:** e24918

Vandesompele J, De Preter K, Pattyn F, Poppe B, Van Roy N, De Paepe A, Speleman F (2002) Accurate normalization of real-time quantitative RT-PCR data by geometric averaging of multiple internal control genes. Genome Biol **3:** RESEARCH0034

Varkonyi-Gasic E, Wu R, Wood M, Walton EF, Hellens RP (2007) Protocol: a highly sensitive RT-PCR method for detection and quantification of microRNAs. Plant Methods **3:** 12

Ye J, Coulouris G, Zaretskaya I, Cutcutache I, Rozen S, Madden TL (2012) Primer-BLAST: a tool to design target-specific primers for polymerase chain reaction. BMC Bioinformatics **13:** 134